Simplifying the Temporal Analysis of Products Reactor

Lilliana Brandão[1], Eric A. High[1,2], Taek-Seung Kim,[1] Christian Reece[1*]

1. Harvard University, Rowland Institute at Harvard, Cambridge, MA 02142, USA
2. Tufts University, Department of Chemistry, Medford, MA 02155, USA

*christianreece@fas.harvard.edu

Abstract

The Temporal Analysis of Products (TAP) experiment provides an unparalleled level of kinetic insight into heterogenous catalytic materials, but due to the complex and expensive instrumentation required, its application has been limited to a small group of dedicated researchers. Herein we demonstrate through a series of designs that precisely defined TAP experiments can be performed on systems far smaller and simpler than previously imagined. The pulse reactors described in this work utilise readily available components and so can be assembled, operated, and maintained with minimal training. Using the case study of CO oxidation over a Pt/SiO_2 catalyst we show that precise kinetic, mechanistic, and surface composition information is feasible using our single-valve design. With the developments outlined in this work we aim to decrease the activation barrier to TAP and open up the technique to a new generation of researchers.

Keywords: Transient Kinetics, Heterogenous Catalysis, Temporal Analysis of Products, Transient Response, CO Oxidation

1. Introduction

The ability to resolve fine kinetic features of heterogenous (gas-solid) catalytic systems is of great importance when it comes to designing new catalysts. By precisely determining reaction mechanisms and kinetic coefficients, it becomes possible to rationalise, predict, and potentially enhance catalytic behaviour [1–3]. Steady-state kinetic studies have been employed extensively and successfully, but they are often limited in their scope, as fine kinetic features can be obfuscated by mass-transport effects, rapid decomposition of intermediates, or by the reaction network collapsing to a small number of rate limiting steps [4,5]. Non-steady-state techniques such as Steady State Isotopic Transient Kinetic Analysis (SSITKA) [6], Molecular Beam Scattering (MBS) [7], or Temporal Analysis of Products (TAP) [8] provide information on time-resolved catalytic activity, circumventing some of the limitations of steady-state experiments. Specifically, the TAP experiment combines the benefits of both SSITKA and MBS experiments as it does not require large amounts of expensive isotopes, can resolve kinetic features with sub-millisecond time resolution, utilises precisely defined transport phenomena [9,10], and bridges the so-called pressure and materials gaps [11]. In particular, the TAP experiment has been successful in elucidating the kinetics for HCl oxidation [12], methanol oxidation [13], and propane dehydrogenation [14], alongside many others [15,16]. Further, due to its molecular level precision, the TAP experiment has more recently found use as a structural/composition characterisation tool [17–19]. However, the significant cost and expertise required to build, maintain, and operate the reactors used to perform the TAP experiment means that even after over forty years of application it has largely been limited to a small number of dedicated research groups, struggling to gain mainstream appeal.

In this work, we demonstrate that precisely defined TAP experiments are achievable in smaller and simpler systems than was previously thought possible. We identify the limiting conditions where TAP experiments transfer out of this precisely defined regime but find that the pulses can still provide in-depth qualitative insight. With this analysis, we aim to reduce the significant activation barrier to TAP experiments and open up the field of transient kinetics to an entirely new generation of researchers.

2. Overview of the TAP experiment

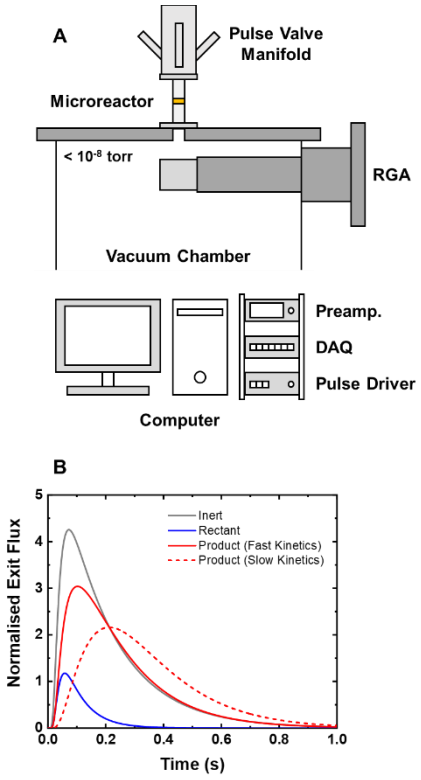

Figure 1. (A) Schematic overview of the pulse reactor used in TAP experiments. (B) Representative TAP exit flux curves for the irreversible adsorption and reaction of a reactant compared to the response of an inert gas. The reactant (blue) is consumed during the pulse to create the product (red) and as such has a decreased magnitude and thinner shape than the inert curve (grey). The product curves for a corresponding fast (solid line) and slow (dashed line) kinetic process show that the shape of the product curve provides insight into the speed at which the surface reaction takes place.

First published by Gleaves in 1988 [20] and refined by Gleaves and Yablonsky in 1997 [8], the TAP experiment, outside of some modernisation and automation [11], has remained largely unchanged in the last 26 years. Approximately 22 groups have worked with TAP reactors, of which, 17 groups use systems developed by Gleaves with an additional 5 groups using home-built versions [21]. All these systems contain the same three components. A pulse valve (or pulse valve manifold), a microreactor containing a powdered catalyst (typically a thin zone of catalyst sandwiched between two layers of inert material), and a Residual Gas Analyser (RGA) that is housed in an ultra-high vacuum (UHV) chamber, all of which are controlled by a computer and external components (Figure 1A). Conceptually the TAP experiment is very simple: a short sharp pulse of gas is sent into the microreactor and the flux of gas at the reactor exit is recorded. When the pulse size is kept small ($< 10^{15} – 10^{16}$ molecules) the transport occurs via Knudsen diffusion. Under these conditions the gas phase interactions are minimised, and the shape of the exit flux curve is defined by the gas-surface interactions, and by extension, the underlying physical and chemical processes. Therefore, by comparing the shape and magnitude of the exit flux curve for a reactant / product to that of an inert gas, detailed kinetic and mechanistic insight into catalytic processes becomes possible (Figure 1B). The exit flux response curves in a TAP experiment are often reported as “normalised exit flux” or “normalised exit flow” which is the measured exit flux/flow normalised to amount of the species in the inlet pulse:

$$F_A^{norm} = \frac{F_A}{(N_A/A)} \quad (1)$$

where F_A^{norm} is the normalised exit flux of A (1/s), F_A is the exit flux of A (mol/cm^2/s), N_A is the number of molecules of A in the inlet pulse (mol), and A is the cross-sectional area of the reactor (cm^2). Products not included in the inlet pulse are normalised to the corresponding reactant inlet pulse.

If the pulse size is sufficiently small that the number of molecules is significantly less than the total number of active sites on the catalyst surface, a single pulse should not modify the catalyst surface by any appreciable amount. Under these conditions, the pulse acts as a *kinetic snapshot* of the catalyst surface at that given state, defined as a *state-defining* [8] experiment (Figure 2A). By repeatedly pulsing, it becomes possible to induce finite changes in the catalyst surface through a series of small infinitesimal steps such that the experiment becomes *state-altering*, known as *chemical calculus* [22] (Figure 2B). By utilising a multi-valve system, it becomes possible to perform a *dynamic state-defining* experiment where a pump molecule is sent into to the reactor, then after a time delay, a probe molecule is sent into the reactor (Figure 2C). The pump and probe pulses should not alter the underlying catalyst state, and by altering the time delay between the pump and probe molecules, this allows dynamic understanding of kinetics at a fixed catalysts state [15]. While the microreactor is at UHV between pulses, during a pulse the pressure over the catalyst in the reactor at the peak of the pulse is in the range of 0.1 – 1 mbar [16], placing the TAP experiment in the same category as other *operando* methods. A more recent development of the technique involves increasing the pulse size such that the transport leaves the Knudsen regime and that gas-gas collisions can occur. This makes it possible to "switch on" gas phase collisions, potentially allowing deconvolution of gas phase and surface reactions [23,24]. The examples referenced here are only a small sample of the applications of the TAP technique, with extensive reviews published elsewhere [11,15,16,25].

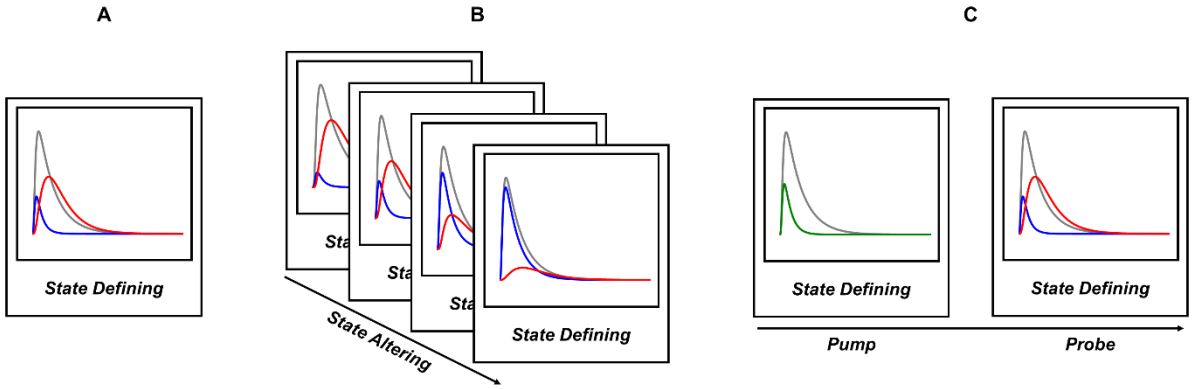

Figure 2. Schematic outlining the three most popular types of TAP experiments. A) In a single pulse experiment, the catalyst surface is unperturbed such that the resulting exit flux acts as a *kinetic snapshot* of the catalyst state. B) By repeatedly pulsing it becomes possible to incrementally modify the catalyst state. By recording a series of snapshots as a function of evolving catalyst state, it is possible to watch the evolution of the catalyst surface. C) By pulsing a pump molecule, followed by a probe molecule after a certain time delay, it is possible to record the evolution of dynamic species on the catalyst surface at a fixed catalyst state.

As a RGA is commonly used to measure the exit flux in a TAP experiment, the pulsing sequence is limited to scanning only one M/Z value for the duration of the pulse. When a pulse experiment is performed under *state defining* conditions, multiple pulses are combined together into a *pulse set* which is then taken as a static catalyst state and is used to calculate reaction kinetics. The pulse set contains

the reactant(s), the inert tracer, and the product(s), which in one of the simplest cases contains three individual pulses (Figure 3), but in more complex cases can consist of many pulses. It's important to note that while the entire suite of chemical processes occur in each pulse, only one species can be recorded at a time. The TAP reactor has been combined with a Time-of-Flight (TOF) mass spectrometer [26] to circumvent the requirement to combine data into a pulse set, but these TAP-TOF instruments have rarely seen application. Unfortunately, the terms pulse and pulse set are often used interchangeably which can cause confusion, but in almost all circumstances TAP exit flux curves are represented in the pulse set format.

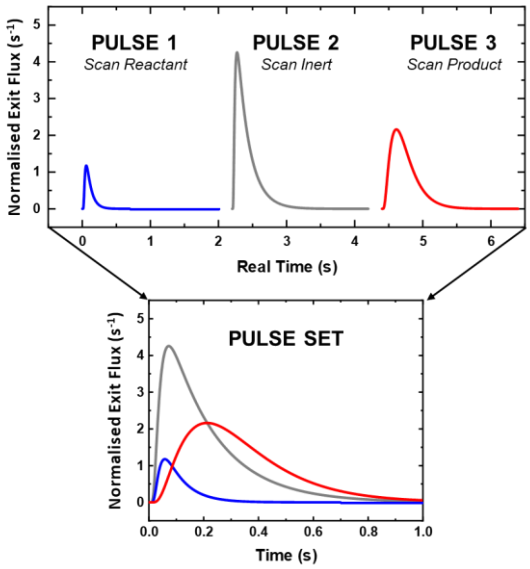

Figure 3. Description of a "pulse set". As most RGAs can only record one mass over the timescale of a pulse, multiple pulses are required to record a single point. In the example shown three pulses (M/Z values) are required to probe the reactant, inert, and the product. These three pulses are then combined to make a pulse set.

3. Defining the TAP model

From simply studying the shape and magnitude of the exit flux curves the TAP experiment can provide in-depth insight into both reaction kinetics and mechanisms. However, it is the precise modelling of the experiment that makes TAP a uniquely powerful kinetic tool for determining rate constants [13,27–29] and mechanisms [23,30]. The exact conditions required for quantitative modelling of the TAP experiment were outlined by Yablonsky in 1997 [8] and are:

1. The governing transport phenomena is Knudsen Diffusion.
2. The pulse size is sufficiently small that the experiment is *state defining*.
3. The transport (and as such, the shape of the exit flux curve for an inert gas) is solely defined by the characteristics of the microreactor's packed bed, with no pre- or post-diffusive zones affecting the shape of the exit flux.

The first two requirements are relatively easy to achieve, and have been implemented in many other TAP-like systems [31–34] but so far only the systems developed by Gleaves [8,11] have ever been shown to rigorously verify the third requirement.

The series of equations and boundary conditions that describe a precise TAP experiment have been discussed extensively in the previous literature [8,9,35,36], but they are summarised here for reference.

The TAP reactor model is often partitioned into *zones*, where each zone represents a different part of the catalyst bed (*e.g.*, inert zone, catalyst zone) with the typical setup being an inert zone, a thin catalyst zone, followed by another inert zone [35]. *It is important to note that the zones in this model all exist within the packed bed of the microreactor*, and that while zones outside of the packed bed may be included in a model, these are poorly defined and difficult to rigorously isolate. For each zone, a one-dimensional diffusion/reaction equation is utilised, which for a reversibly adsorbing gas is:

$$\varepsilon_b \frac{\partial C_A}{\partial t} = D_{eA} \frac{\partial^2 C_A}{\partial z^2} - \alpha_s S_V (1 - \varepsilon_b)(k_a C_A \theta_* - k_d \theta_A) \tag{2}$$

where ε_b represents the void fraction of the reactor, C_A represents the concentration of the gaseous species A (mol/cm^3), t is the time relative to the triggering of the pulse (s), D_{eA} is the effective Knudsen diffusivity of gas A (cm^2/s), z is the axial coordinate of the reactor (cm), α_s is the concentration of active sites on the catalyst surface (mol/cm^2), S_V is the surface area of catalyst per volume of catalyst (cm^2/cm^3), k_a is the adsorption rate constant (cm^3/mol/s), θ_* is coverage of free sites, k_d is the desorption rate constant (1/s), and θ_A is coverage of adsorbed A. For noninteracting cases (*i.e.*, over inert packing) the terms relating to the kinetics are set to zero, such that only diffusion occurs. Most commonly, the surface species are modelled using a mean-field microkinetic model, which for the reversibly adsorbing species would be:

$$\frac{\partial \theta_A}{\partial t} = k_a C_A \theta_* - k_d \theta_A \tag{3}$$

When gas travels between two zones within the packed bed, both flux and concentration are conserved such that:

$$C_A^n(1, t) = C_A^{n+1}(0, t) \tag{4}$$

$$- D_{eA}^N \frac{\partial C_A^n}{\partial z}(1, t) = - D_{eA}^{N+1} \frac{\partial C_A^{n+1}}{\partial z}(0, t) \tag{5}$$

for a given zone n the concentration of A and the flux of A conserved when transitioning to from zone n to zone $n + 1$. For a gas being pulsed into the reactor the initial condition is defined as:

$$C_A(z, 0) = \delta(z, 0) \tag{6}$$

where $\delta(z, 0)$ represents a delta function introduced into the reactor inlet at a time t = 0. After introducing the pulse into the microreactor, the pulse valve is closed, and so the boundary at the entrance to the packed bed can be defined as:

$$\frac{\partial C_A(0,t)}{\partial z} = 0 \tag{7}$$

As the exit of the microreactor is attached to a vacuum, the exit condition at the end of the packed bed is defined as:

$$C_A(L,t) = 0 \tag{8}$$

where L is the total length of the reactor (cm). Finally, the flux of gas leaving the reactor, which recorded during the experiment, is defined as

$$F_A = -D_{eA}\frac{\partial C_A(L,t)}{\partial z} \tag{9}$$

Generalised analytical solutions exist for first-order (or pseudo first-order) state defining experiments [9,35,37,38], with numerical simulation utilised for non-linear experiments [13,39,40].

4. The Gleaves TAP system design

The TAP systems developed by Gleaves have been described extensively in the previous literature [8,15,25] but the core components are highlighted here. The TAP-2 (and TAP-3) systems consists of an oil diffusion pump (e.g., Varian VHS-10) that is mounted to a large liquid nitrogen cooled chamber that can be isolated from the rest of the system using a gate valve. A vacuum chamber containing a turbomolecular pump (e.g., Varian Turbo-V70) and an RGA (e.g., Stanford Research Systems RGA300) is attached to the other side of the gate valve. A custom-built microreactor is attached to the top of the vacuum chamber via an O-ring seal, which can be isolated using a slide valve assembly, allowing the user to rapidly change samples. The inclusion of a vent line and needle valve within the slide valve assembly also allows the user to perform atmospheric pressure flow treatments of catalysts by flowing gas through the pulse valve manifold with the gas being sampled by the RGA using the needle valve. Finally, a pulse valve manifold containing multiple (2-4) solenoid valves and a continuous flow valve is mounted above the system, which can be lowered and raised as needed (Figure 4A). During operation the pulse valve manifold is lowered and sealed to the microreactor via an O-ring, the liquid nitrogen cooled chamber is filled, the gate valve is opened, and then the microreactor is exposed to the vacuum (~1×10^{-8} torr base pressure) via the slide valve assembly.

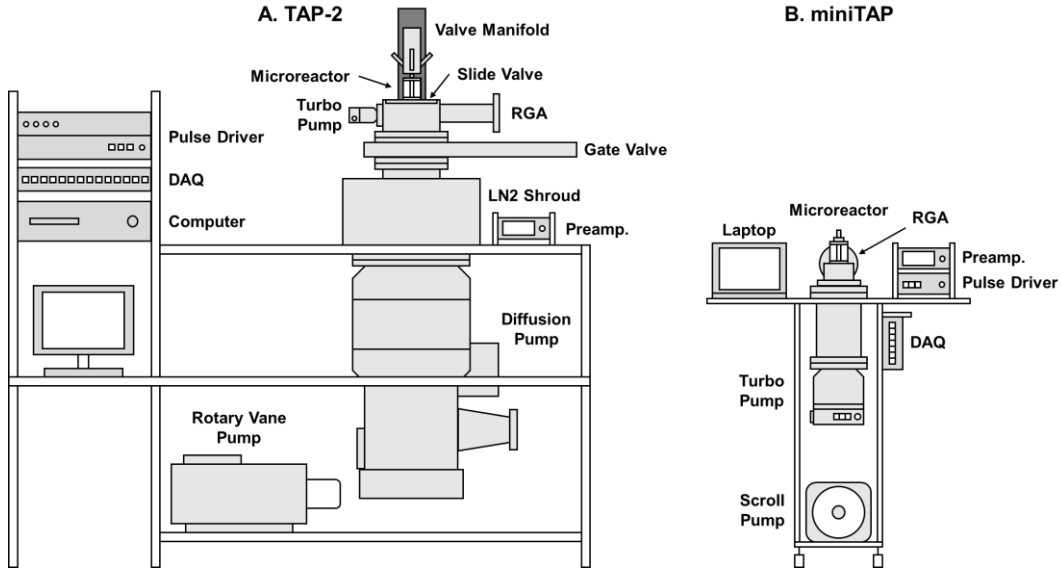

Figure 4. Schematic illustration of A) The TAP-2 system developed by Gleaves and B) The miniTAP developed as part of this work. Drawings are approximately to scale.

The Gleaves system has been specifically designed so that at the entrance of the packed bed the flux is zero, and at the exit of the packed bed the concentration is zero and only the exit flux is being measured (equations 6 and 7). Practically speaking what these two terms relate to is that there should be no measurable pre-volume before the packed bed in which gas can reside (Figure 5A), and that once the gas leaves the microreactor and enters the vacuum chamber it should be instantaneously detected by the RGA and then pumped out such that it does not reside in the chamber and get detected multiple times (Figure 5B). To remove the pre-volume, custom solenoid valves with extended stems were designed such that the tips of the valve stems met at the exit of the pulse valve manifold [8]. To ensure that the gas was instantaneously detected after leaving the microreactor, the RGA was mounted so that the filament and ioniser were directly below the exit of the microreactor (which also has the added benefit of significantly increasing detection sensitivity). Finally, to ensure that any gas leaving the microreactor was not backscattered and only detected by the RGA once, the vacuum is generated using a high pumping speed oil diffusion pump (> 3500 L/s pumping speed) and the top chamber was differentially pumped using a small turbomolecular pump (70 L/s pumping speed).

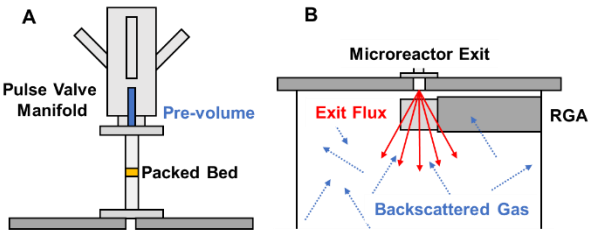

Figure 5. Schematic representations of the two limiting conditions for well-defined TAP experiments. A) That no pre-volume exists before the packed bed in the microreactor such that it acts as an extra "zone" within the TAP model. B) That when the gas exits the microreactor it is instantaneously detected and pumped away so that no backscattering gas exists that can be detected by the RGA.

While the Gleaves system's capabilities are highly desirable, the increased complexity of the design meant that it took a significant level of skill to operate and maintain the system and perform the TAP experiment. The bespoke nature of many of the parts in the system meant that it was not simple to fix and/or replace the components as they age. Further the oil diffusion pump meant that contamination of the vacuum components (e.g., the RGA) with residual pump oil would cause shortened lifespans and

drifting signals. This resulted in the TAP technique having a significant barrier to entry as reliable operation requires a highly trained and dedicated user. To rectify these issues, we have designed a simplified TAP reactor system that is oil free and consists of minimal components all of which are readily available.

5. Simplifying and Miniaturising the TAP reactor

In an effort to simplify the TAP reactor we have developed the miniTAP (Figures 4B, S1, 8B) which was influenced by both the Gleaves TAP-2 design [8] and the Delft TAP (Multitrack) system [33]. When designing the miniTAP reactor four core principles were laid out:

1. All components must be commercially available or easily sourced.
2. All components must be easy to repair and/or replace if damaged.
3. The system should be operable with minimal training.
4. The system must contain minimal contaminants to ensure consistent results.

5.1 The Vacuum system. The miniTAP consists of a medium sized turbomolecular pump (Pfieffer HiPace 700, ~700 L/s pumping speed) that is connected to a standard DN160CF nipple (9" OAL). A DN160CF to DN35CF reducer tee could also be used to mount a pressure gauge if desired. The use of a turbomolecular pump coupled with a dry scroll pump (Edwards XDS 5) means that the vacuum chamber remains oil free (minimising contaminants) and can reliably reach base pressures << $1x10^{-9}$ torr during operation. The contaminant free operation of the system means that consistent signals in the RGA are possible over the course of weeks to months, with little re-calibration of the system required. The nipple is attached to a DN100CF "hat" which has a DN63CF arm in the correct orientation so that an RGA can be mounted directly beneath the microreactor exit (Figure S2). The microreactor utilised is based on the Gleaves TAP-2 design (Figure S3.1). A quartz tube (6.35 mm OD, 4 mm ID) is connected to a modified DN35CF ConFlat flange which contains a removable stainless screen to hold the packing in place and is sealed via an O-ring (Kalrez, -010). The top of the microreactor is a custom-built assembly that is also connected to the quartz tube via O-ring that has a small 0.020" side hole that allows a thermocouple to be fed through into the packed bed. The top of microreactor also has a 4 mm ID opening so that the packing is extended all the way to the top of the microreactor. A solenoid pulse valve (Parker Miniature High-Speed Vacuum Valve) is directly mounted to the top of the microreactor assembly which is also sealed using an O-ring (Figure S3.2). The reactor is packed upside down and is designed so that the packing extends all the way to the exit of the pulse valve. A small extension cylinder is also attached to the vacuum side of the microreactor to assist directing the exit flux to the RGA (Figure S3.3). The vacuum chamber, turbopump and pulse valve are standard parts, that are attainable without any modifications from commercial sources. The "hat" uses standardised vacuum components that can be readily assembled by any vacuum company. Finally, while the microreactor consists of bespoke machined components, we have found that acceptable quality and tolerances for all of the parts was attainable using online machine shops.

The miniTAP system does lack some of the benefits of the Gleaves design. First, the removal of the slide valve means that it is not possible to isolate the microreactor from the vacuum equipment for rapid sample transfer or atmospheric pressure pre-treatments. We consider this an acceptable loss as sample transfer is rarely the time-limiting factor in TAP experiments. Further, we have found that atmospheric pressure pre-treatments can be mimicked by turning off the RGA and sending large pulses of pre-treatment gas through the reactor. Second, the lack of a multi-valve system means that pump-probe experiments are not possible. While many would find this a significant drawback of the miniTAP system, experiments that can be precisely modelled using analytical functions such as single pulse, multi-pulse, and titration style experiments are still accessible (see section 7). Further, other groups [23,33] have successfully designed a multi-valve manifold with minimal pre-volume using commercial

solenoid valves. Finally, the use of a turbomolecular pumping system can cause problems with efficiently pumping hydrogen from the vacuum system. While we do find that hydrogen does not fit the idealised pulse response shape (see section 6, Figure S4) we see no significant build-up of H_2 base pressure during our experiments. Further, due to water (and all hydrocarbons) containing a cracking fragment at M/Z of 2 any precise modelling of the H_2 pulse shape is often not feasible due to the imperfect nature of subtracting cracking fragments.

5.2 The Pulsing System. In order to correctly perform a TAP experiment, the pulsing system must be able to precisely time the simultaneous triggering of the valve and data collection, such that the valve opening can be aligned to $t = 0$. Further, as the reactant and product curves are normalised to the inert tracer during each pulse set (Figure 3), the pulsing system must also be designed such that the pulse-to-pulse deviation is minimised. For valve firing and data acquisition a number of systems have already been developed. The Gleaves systems combines the custom built solenoid pulse valve manifold with a home-built driver [8,11] with the timing, triggering, and data collection performed using commercial DAQ devices (National Instruments) controlled using home-built LabVIEW software. The system developed at Delft University [33] uses a custom pulse valve manifold that houses multiple commercial ultra-high speed solenoid valves (Parker Series 9) that are triggered using the corresponding commercial driver (Parker IOTA One), with the timing performed using a commercial DAQ device (National Instruments). A system at Ulm University [32] opted for custom piezoelectric valves [41,42] driven by home-built electronics that are controlled using LabVIEW software. All systems report pulse-to-pulse deviations between 2-8%, which allows for consistent collapsing of the data into pulse sets.

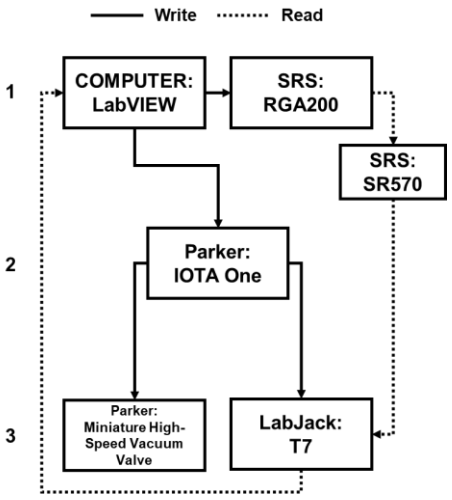

Figure 6. The workflow and components utilised in this work for performing a TAP Experiment. Solid lines indicate writing of data, with dashed lines indicating the reading of signals or data.

The workflow and components for a pulse experiment used in this work are outlined in Figure 6 and follows a three-step procedure. First, the computer sets the RGA (Stanford Research Systems RGA200) to the desired M/Z value to be recorded during the pulse. The selection of RGA is highly important, and two systems were tested as part of this work: a Hiden 3F PIC and the Stanford Research Systems (SRS) RGA200 both of which have been used in TAP systems developed by Gleaves [25]. It was found that the radial asymmetry that is present in the Hiden 3F PIC ioniser caused the signal response to be modified as a function of RGA orientation, whereas the SRS RGA200 is radially symmetric, and orientation had no effect on the signal. The SRS RGA200 also has the benefit of being lower cost while maintaining a wide dynamic range of detection, and also being simpler to interface with via freely available LabVIEW drivers. Based on the four core principles outlined earlier for the development of the miniTAP it was decided that the SRS RGA200 was the optimal RGA for this system.

In the second step, after a short settle time required by the RGA to allow the M/Z value to be set, the computer simultaneously records a timestamp and sends a command to the pulse valve driver (Parker IOTA One) to initiate the pulse. The commercial pulse valve driver was found to be able to reliably generate pulses with < 3% pulse-to-pulse deviation (Figure 7A) similar to other systems and was able to vary the pulse intensity with microsecond precision (Figure 7B) with typical operation in the ~105 µs range. It should be noted that we have found that the pulse width required to get an equivalent pulse size will vary slightly from valve to valve (and even from driver to driver). The pulse valve driver is simple to interface with using standard serial communication in LabVIEW, and outputs a corresponding +5V TTL signal when the valve is triggered. The Parker IOTA One driver has also been successfully used in the Delft TAP system [33]. While the driver is easily sourced, it remains one of the most expensive components in the miniTAP system, meaning that, if possible, a home-built driver may be more optimal.

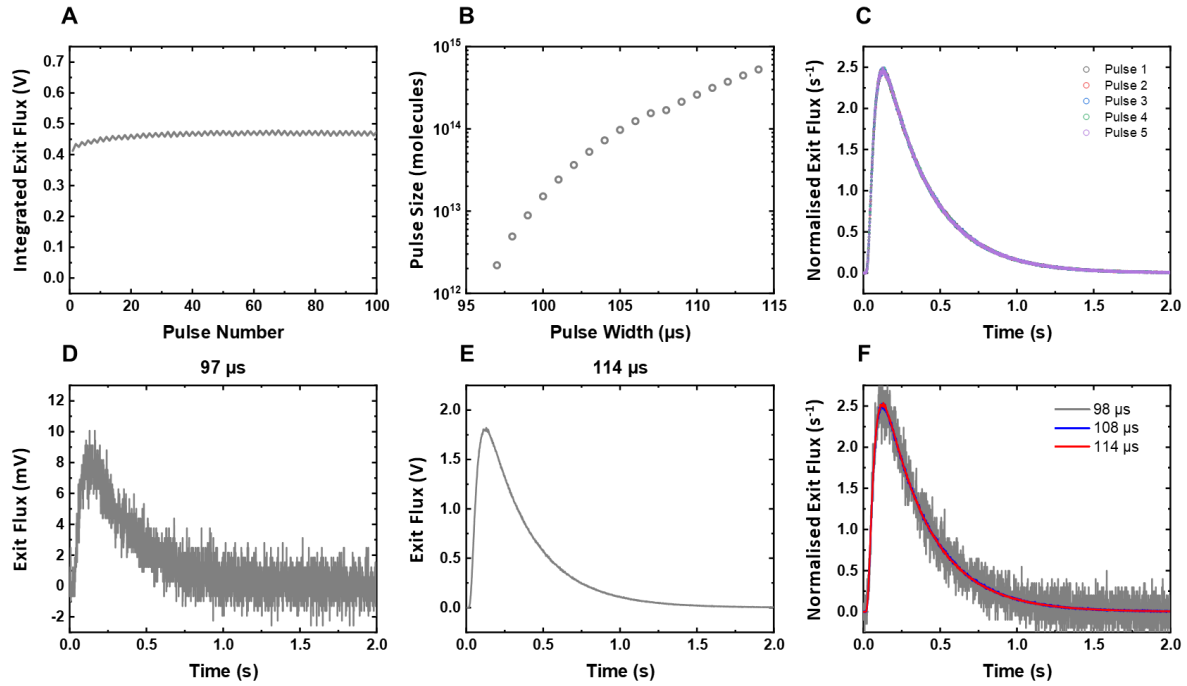

Figure 7. Characterisation of the pulsing system used in miniTAP. A) Integrated raw signal as a function of pulse number for Ar pulsing at 108 µs. B) Pulse size as a function of pulse width. C) Overlayed normalised exit flux for 5 Ar pulses at 108 µs pulse width. D) Raw signal for a single pulse of Ar with a pulse width of 97 µs. E) Raw signal for a single pulse of Ar with a pulse width of 114 µs. F) Normalised exit flux for pulses ranging from 98 – 114 µs. Pulses are consistent with < 3% pulse-to-pulse deviation and no change in pulse shape. Signals across 200x dynamic range are clearly measurable and no change in pulse shape occurs with increasing pulse intensity.

In the final step, upon receipt of the command from the computer, the pulse valve driver simultaneously fires the pulse valve (Parker Miniature High Speed Vacuum Valve) and triggers the data collection on the data acquisition (DAQ, LabJack T7) device. The Parker Miniature High Speed Vacuum (MHSV) valves pair easily with their corresponding drivers (Parker IOTA One) and require no external tuning or modification. The valves are simple to repair, but we have found that the operational lifetime of the valve when used with the IOTA One driver is significant such that a single valve has been used for > 3 years for > 100 K pulses with no maintenance or drifting of the pulse intensity. The synchronisation and normalisation of the data (such that $t = 0$ is set upon receipt of the trigger) is all performed by the LabJack T7 DAQ device. The LabJack can be triggered in "stream" mode using the external 5V TTL signal from the IOTA One, which is reliably triggered so that $t = 0$ is consistently set between pulses (Figure 7C). The LabJack will then sample the corresponding stream at

the pre-set frequency with minimal noise. The LabJack also interfaces to the computer via freely available LabVIEW drivers. The signal from the RGA is first passed through a SRS SR570 current preamplifier set to 100 nA/V gain, high bandwidth mode, with a 300 Hz 6dB lowpass filter. Extreme care must be taken when using a current preamplifier, as if the bandwidth of the preamplifier is sufficiently low it can broaden the exit flux response, causing misinterpretations of results. Other current preamplifiers (Ithaco 2111, Keithly 427) were also tested, but it was found that the SR570 provided the highest signal to noise when paired with the SRS RGA200, providing > 200x dynamic range of detection (Figure 7D-F) at a fixed gain with no change in pulse shape. Once the signal from the preamplifier has been recorded by the DAQ device for the given collection time, the recorded data is sent to the computer and is saved and exported. The pulsing sequence can then be repeated as many times as desired.

6. Confirming the TAP experiment

As part of this work, three TAP systems were developed utilising the same core components as the miniTAP. First, the simpleTAP (Figure 8A) was built, which uses a large turbomolecular pump (Edwards STP iX3006C, 3000 L/s pumping speed) that is connected to a DN250CF nipple (20.5" OAL) which is connected to a DNCF200 hat chamber. The simpleTAP was developed to be analogous in size and pumping efficiency to the Gleaves TAP system, but instead uses a turbomolecular pump and the simplified pulsing system. Second, the miniTAP (Figure 8B) was built which has been described in the previous section. Finally, the microTAP (Figure 8C) was built which uses a small turbomolecular pump (Edwards nEXT 300D, 300 L/s pumping speed) that is connected to a standard DN100CF nipple or DN100CF to DN35CF reducer tee (8.5" OAL) and uses the same DN100CF hat as the miniTAP. The goal was to identify if precisely defined TAP experiments were feasible on simplified turbomolecular pumping systems, and if so, to identify the minimum pumping speed required to ensure that the precisely defined TAP conditions can be met.

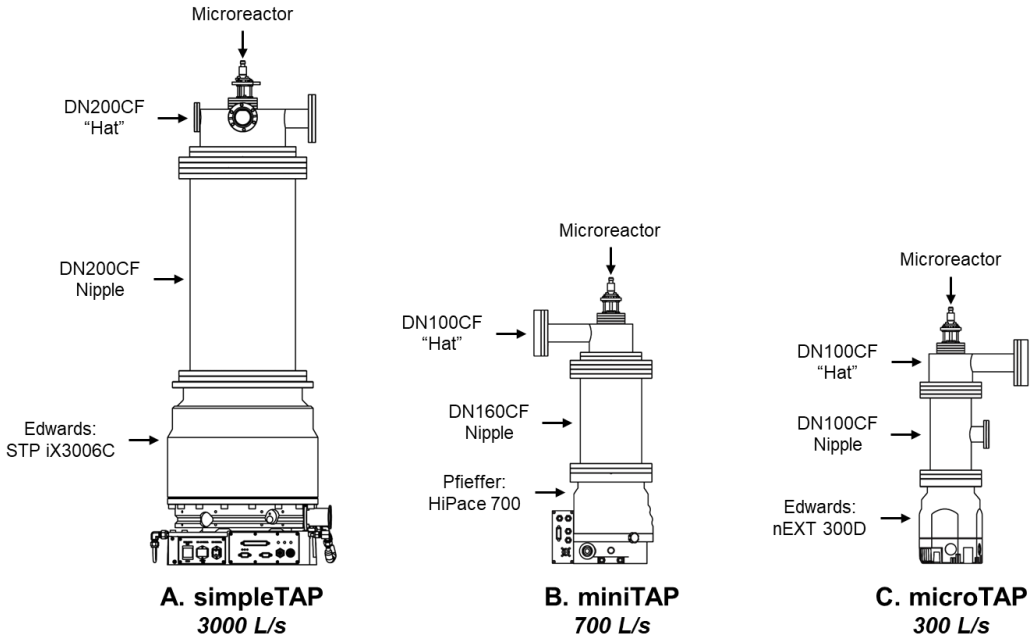

Figure 8. The three TAP systems developed as part of this work. A) The simpleTAP which uses a large 3000 L/s turbomolecular pump. B) The miniTAP which uses the medium sized 700 L/s turbomolecular pump. C) The microTAP which uses a small 300 L/s turbomolecular pump. All TAP systems utilise the same pulsing system and microreactor.

To ensure that the exit flux curves can be precisely defined, the three characteristics outlined by Yablonsky in 1997 must be met (see section 3). The first characteristic is that: *The governing transport phenomena is Knudsen Diffusion.* The requirements are that the pulse size is sufficiently small that only diffusive transport occurs which typically requires pulse sizes in the range of $\leq 10^{16}$ molecules per pulse. This has the added benefit of also enforcing condition two: *The pulse size is sufficiently small that the experiment is state defining.* The pulse size can be reliably calculated by simply pulsing gas from a small fixed pre-defined volume and measuring the pressure drop as a function of pulse number. By isolating the valve and continuously pulsing Ar, the pulse size in our system under typical pulsing conditions was determined to be ~$5x10^{14}$ molecules per pulse (Figure 7B). However, to confirm Knudsen Diffusion is the primary transport phenomena two parameters can be used. First, the pulse shape must be independent of the size of the pulse (Figure 7F), and second, the mean residence time of the reactor must be linearly dependent on the mass and the temperature. For a noninteracting gas (e.g., an inert gas, or a reactive gas through a bed packed with inert powder) equation 1 can be redefined using:

$$\varepsilon_b \frac{\partial C_A}{\partial t} = D_{eA} \frac{\partial^2 C_A}{\partial z^2} \tag{10}$$

with the Knudsen Diffusivity being linearly dependent on the mass and temperature of the gas through the following relationship [43]:

$$D_{eA} = \frac{\varepsilon_b d_i}{3\tau} \sqrt{\left(\frac{8RT}{\pi M}\right)} \approx \sqrt{\frac{T}{M}} \tag{11}$$

where d_i is the diameter of the interstitial voids (cm), τ is the tortuosity (cm/cm), T is the temperature (K), and M is the molar mass of the gas (kg/mol). The mean residence time (t_{res}) in the reactor can be calculated by taking the ratio of the first moment to the zeroth moment for the exit flux response, and is correlated to the Knudsen Diffusivity in a TAP system via the following relationship [8,44]:

$$t_{res} = \frac{M_1}{M_0} = \frac{\int_0^\infty tF(t)\,dt}{\int_0^\infty F(t)\,dt} \approx \frac{1}{D_{eA}} \approx \sqrt{\frac{M}{T}} \tag{12}$$

Therefore, if Knudsen diffusion is present, and the bed is noninteracting, the residence time of the gas is linearly dependent on the mass of the gas and the temperature of the bed. As there are often minor temperature gradients in the TAP reactor system, the linear relationship with temperature is often less well defined, therefore the temperature was fixed at 100 °C for the simpleTAP and room temperature for mini and microTAP experiments and only the mass of the gas was varied. The increased temperature for the simpleTAP measurements was due to normalisation with a separate set of data and does not affect the discussion here. In Figures 9A-C the residence time for a series of gases (H_2, Ne, N_2, O_2, Ar, CO_2, Kr, Xe) pulsed through a microreactor packed with sand (sieved between 50-70 mesh, 5.881 cm length, 0.464 void fraction) as a function of mass are recorded. For all reactors we find that Knudsen diffusion is the primary transport mechanism as a precise linear relationship between the residence time and the mass of the gas was found (Figures 9A-C). Some minor deviation from the linear relationship was seen for CO_2 which we prescribe to some small interaction between CO_2 and the sand, as at higher temperatures the deviation was removed.

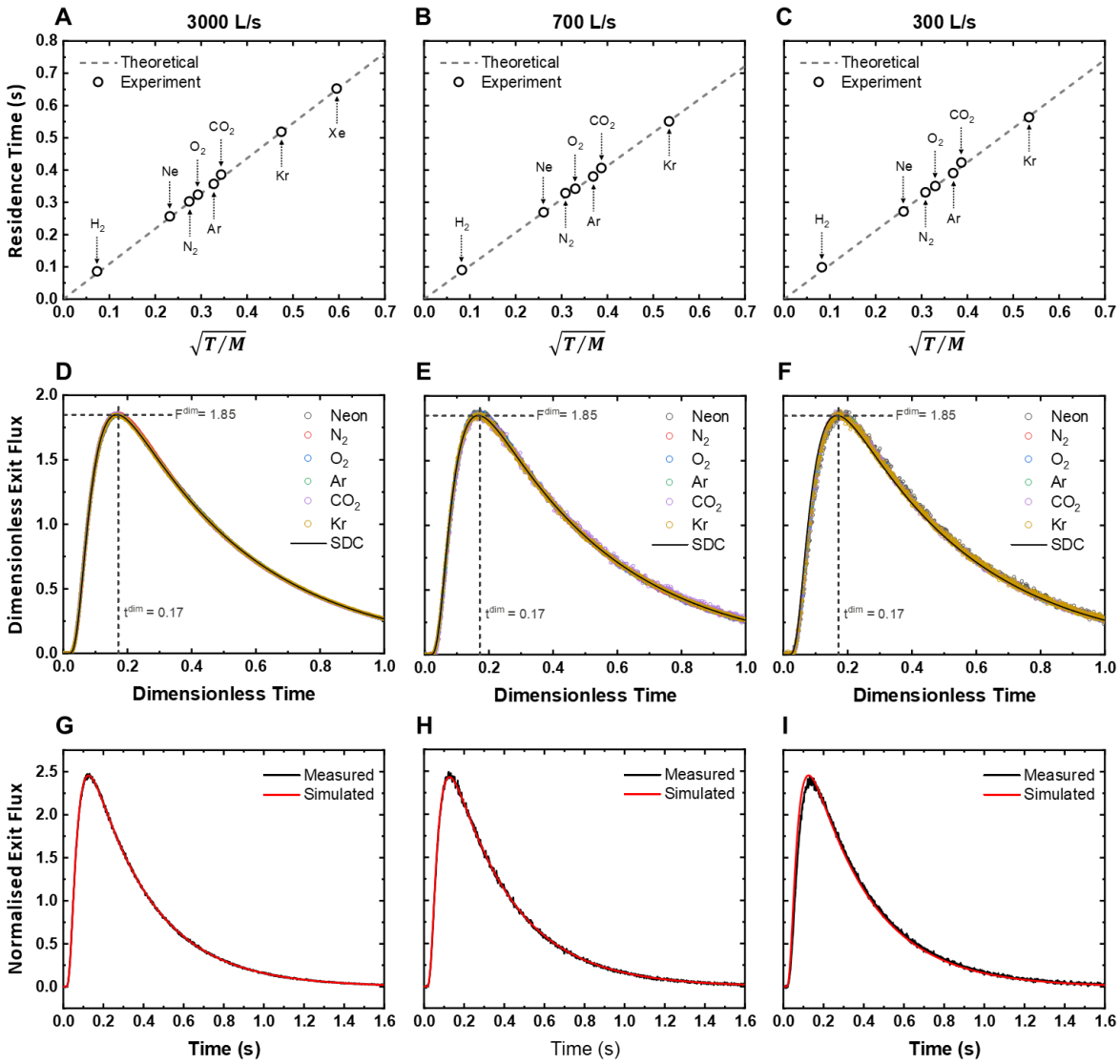

Figure 9. A-C) Mean residence time recorded as a function of the mass and temperature of the gas. The theoretical curve is calculated by scaling the residence time measured for Argon at room temperature. D-F) Dimensionless exit flux curves plotted against the standard diffusion curve (SDC) with the key time and flux characteristics overlayed. G-I) Normalised exit flux compared to the fit of a one-zone (1Z) model. All exit flux curves were taken as the average of 5-10 curves to minimise noise. All pulses were performed using the same microreactor packed with sand (sieved between 50-70 mesh). Pulses were performed using the A), D), G) SimpleTAP, B), E), H) miniTAP, and C), F), I) microTAP systems. Knudsen diffusion is the dominant transport phenomena in all systems tested, but only for the simpleTAP and miniTAP systems was the transport solely defined by the packed bed of the microreactor.

After confirming that Knudsen diffusion is the primary transport mechanism in the reactor, the final step to confirm if quantitative modelling of the TAP experiment is possible is to check if condition 3 is met: *The transport (and as such, the shape of the exit flux curve for an inert gas) is solely defined by the characteristics of the microreactor's packed bed, with no pre- or post-diffusive zones affecting the shape of the exit flux*. In order to confirm that the transport is solely defined by the microreactors packed bed, two checks can be made. First, the microreactor must be packed in the "one-zone" configuration which is when the packed bed consists of solely a uniform sized inert powder. Next, the exit flux curves for pulses through the "one-zone" reactor can then be converted to dimensionless exit flux and dimensionless time as defined by Yablonsky [8]:

$$F_A^{dim} = F_A^{norm}\, 2t_{res} \tag{13}$$

$$t_A^{dim} = \frac{F_A^{norm}}{2t_{res}} \tag{14}$$

where F_A^{dim} is the dimensionless exit flux of A, and t_A^{dim} is the dimensionless time for species A. When plotted in dimensionless exit flux and dimensionless time, all the exit flux curves for a noninteracting packed bed collapse down to a "master" curve independent of mass and temperature. For a one-zone reactor the master curve has very well-defined properties and is known as the Standard Diffusion Curve (SDC) [8]. First, in the SDC the time of maximum intensity occurs at a dimensionless time of 0.17, and the maximum intensity of the dimensionless exit flux is 1.85. Any deviation from the SDC (while under Knudsen Diffusion conditions) can be directly related to the effect of pre- or post-diffusive zones on the shape of the exit flux. The exit flux curves used in the residence time experiment (Figures 9A-C) were converted to dimensionless exit flux and dimensionless time using equations 13 and 14 and are shown in Figures 9D-F. For the simpleTAP and miniTAP cases, the dimensionless curves lie exactly on the SDC, but for the microTAP system there is a slight delay between the measured dimensionless curves and SDC. This would indicate that some pre- or post-diffusive zone exists in the microTAP system. As the same microreactor and pulse valve is used in all three systems, we attribute this right-shifting of the response to a post-diffusive zone. This most likely arises as the small turbomolecular pump (300 L/s pumping speed) used in the microTAP is not sufficient to remove the gas from the system without it being backscattered (Figure 5). For all systems, the dimensionless exit flux curve for H_2 did not lie on the SDC (Figure S3) which was expected due to the difficulty that turbopumps have with pumping H_2, but as mentioned previously this is not considered a large downside due to the imprecise nature of the M/Z 2 response.

The final confirmation that the transport is solely defined by the microreactors packed bed can be made by fitting a model "one-zone" exit flux curve to the experimental data. The analytical form of the one-zone model in the Laplace domain has been derived as [9]:

$$F_{exit}(s) = \frac{1}{cosh\sqrt{st_{res}}} \tag{15}$$

It is possible to express the Laplace function in the Fourier domain via the following relationship [45]:

$$s = \omega i \tag{16}$$

where:

$$\omega = \frac{2k\pi}{t_{max}} \tag{17}$$

with t_{max} being the sampling time (s) of the TAP pulse, and where:

$$k = \frac{-ft_{max}}{2} \ldots + 1 \ldots \frac{ft_{max}}{2} \quad (18)$$

Where f is the sampling frequency of the pulse (Hz). The full derivation of these equations is far outside the scope of this paper, but Equation 16 can then be inserted into equation 15 and the curve simulated in the Fourier domain, which can easily be converted into the time domain using an inverse Fast Fourier Transform algorithm. Using MATLAB, the one-zone model was fit to the normalised exit flux curves for an Argon pulse in each reactor system by varying t_{res} using the nonlinear least-square fitting function fmincon. The exit flux curves (and corresponding model fit) are shown in Figures 9G-I. It was found that the model is able to precisely recreate the normalised exit flux curves for Argon in the simpleTAP and the miniTAP reactors using the same simulated curve. However, for the microTAP reactor the same simulated curve from the simpleTAP and miniTAP reactors does not match the experimental exit flux.

Based on the evidence from the residence time scaling, dimensionless exit flux, and the model fitting, the simpleTAP and miniTAP reactor systems fulfil all three requirements for the quantitative modelling of TAP experiments. We find that the microTAP reactor contains a post-diffusive zone, which means that it can still be used for TAP experiments qualitatively but cannot be used for quantitative modelling using currently existing methods in the TAP community. While this limits the scope, due to the primary transport method being Knudsen diffusion, qualitative insight into reaction kinetics is still possible as all the dimensionless curves collapse onto each other (Figure 9F). Further, due to the molecular level precision the microTAP can still be utilised for compositional site counting. The reactors in this work empirically demonstrate that the TAP experiment and modelling can be performed on systems much smaller and simpler than was previously imagined. Contrary to popular thinking, large pumping speeds and large vacuum systems are not required for the TAP experiment. From our development of the TAP systems in this work we have found anecdotally that excess volume can instead negatively affect the TAP pulse shape. When the simpleTAP was extended with a DN250CF nipple to increase the total volume of the vacuum chamber, we found that the pulse response was broadened, indicating that a post-diffusive zone was generated. Further, when the linear nipple was replaced with a spherical vacuum chamber to increase the volume, broadening was also detected. We postulate that the geometry and the aspect ratio of the vacuum system are instead more important, although we should note that these experiments were not performed methodically due to time and monetary constraints. As the deviation between the SDC and the dimensionless miniTAP curves is only minimal, it could be hypothesised that a microTAP system with precisely the correct geometry and aspect ratio could be designed such that no post-diffusive zone exists, but we were unable to design such a system.

7. Application of the simplified TAP reactors

Although the TAP systems developed as part of this work utilise a single valve setup, through multi-pulse titration experiments precise kinetic and compositional information about catalytic systems is possible. By pre-covering a catalyst in a probe reagent (e.g., CO) and titrating it off with a reactant (e.g., O_2) it becomes possible to simultaneously probe the intrinsic kinetics of different sites, while also quantifying their distribution on the surface. To demonstrate this capability, CO was preadsorbed over a Pt/SiO_2 (2 nm nanoparticle size, 0.7% Pt weight loading) catalyst at 80 °C and the resulting CO was sequentially titrated using O_2 pulsing at 80 °C (Figure 10A). The full details relating to the catalyst synthesis, characterisation, and modelling used here are provided in our previous publication [19]. As the preadsorbed CO is consumed by the O_2 pulses it becomes possible to generate a *kinetic snapshot* (Figure 2) of the CO oxidation reaction across the entire range of CO coverages probed in the titration

experiment. Assuming a stoichiometry of 1 CO_2 molecule produced by each adsorbed CO molecule, the relative CO coverage can be approximated by counting the total amount of CO_2 produced [17,19,29]. By fitting a model to each individual pulse set throughout the experiment, the precise kinetics of the irreversible reaction of O_2 with adsorbed CO as a function of CO coverage and the amount of CO_2 produced by each pathway can be resolved.

Table 1. Pathways included in the three-pathway model for irreversible adsorption/reaction of O_2 with the CO covered 2nm Pt/SiO_2 catalyst. The apparent adsorption/reaction constant is represented by $k'_{a,n}$ and the intrinsic reaction constant for the surface reaction step is denoted by $k_{r,n}$ where *n* is the number of each pathway. IS represents an intermediate surface species.

Pathway	$k'_{a,n}$		$k_{r,n}$		
1	O_2	→	IS1	→	CO_2
2	O_2	→	IS2	→	CO_2
3	O_2	→	$2O^*$		

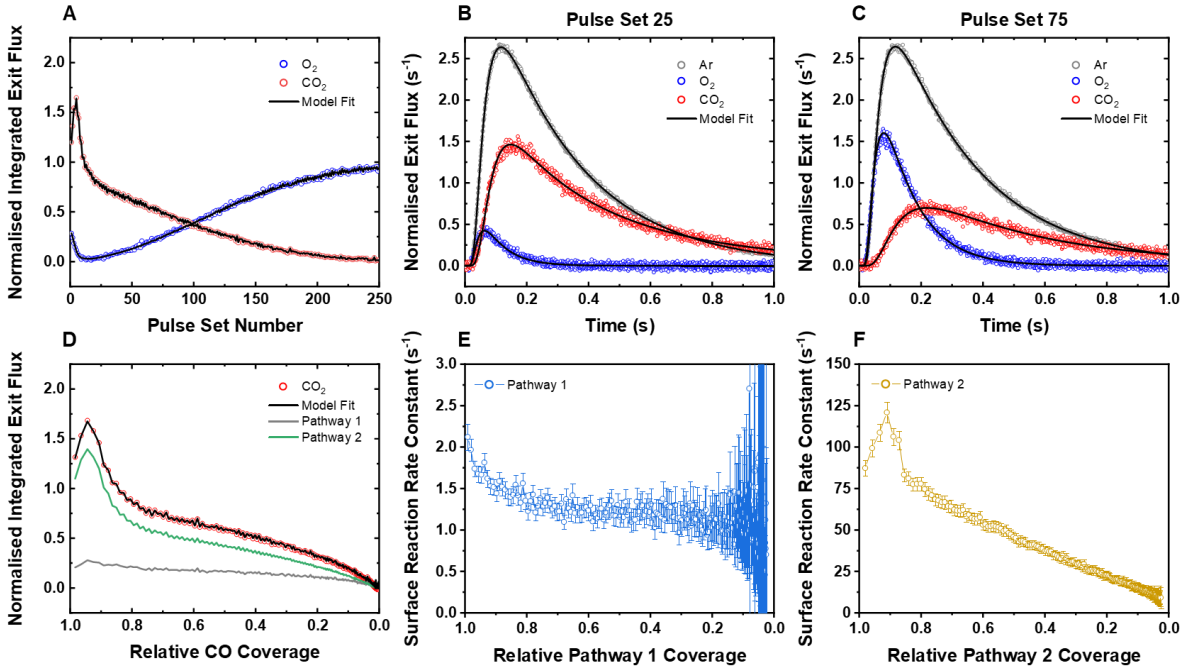

Figure 10. Results from fitting the three-pathway model to the titration experiment where preadsorbed CO on a Pt/SiO_2 catalyst was sequentially reacted off with O_2 pulsing at 80 °C. A) The integrated normalised exit flux recorded for O_2 and CO_2 (open circles) and the corresponding model fit (solid line). B-C) Exit flux curves for Ar, O_2, and CO_2 and their corresponding model fit using the three-pathway model. D) Deconvoluted CO_2 production from each pathway as a function of relative CO coverage. E-F) The surface reaction rate constants and corresponding 95% confidence intervals (kr_1 and kr_2 respectively) for pathways 1 and 2 as a function of their respective coverages.

In our previous work, we identified two pathways for the reaction of adsorbed CO with gaseous O_2 over the 2 nm Pt/SiO_2 catalyst [19]. A fast pathway, which we have correlated to well-coordinated CO binding sites (e.g., terrace sites), and a slow pathway, which we have correlated to under-coordinated CO binding sites (e.g., edge sites) respectively. A third pathway for the irreversible adsorption of O_2 was also included in the model (Table 1). To calculate the kinetics, first a Thin-Zone TAP reactor model was generated using Multi-Zone TAP Reactor Theory [9,19,37] and that model was fit to the exit flux curves of every single pulse set in the experiment (Figures 10B, 10C). All data processing and

regression was performed in the MATLAB programming environment using the lsqcurve fit function, with the 95% confidence intervals estimated using the nlparci function.

Using the calculated kinetic coefficients, it becomes possible to deconvolute the O_2 conversion from each pathway in each pulse set with the following relationship [19]:

$$X_{O_2,n} = \frac{k'_{a,n}\left(L/2D_{eO_2}\right)}{1 + \left(k'_{a,1} + k'_{a,2} + k'_{a,3}\right)\left(L/2D_{eO_2}\right)} \quad (19)$$

Where $k'_{a,n}$ is the adsorption/reaction rate constant for pathway *n*. By applying a carbon balance of 2 CO_2 molecules produced per O_2 consumed, it is simple to then calculate how much CO_2 is produced by the under-coordinated sites (pathway 1) and the well-coordinated sites (pathway 2) individually (Figure 10C). By summing the total amount of CO_2 produced by each pathway the ratio of sites can be calculated. For the 80 °C titration experiment we find that 29.1% of the sites are under-coordinated and 70.9% of the sites are well-coordinated. Interestingly, this is close to the ratio expected for a ~2 nm truncated icosahedron shaped nanoparticle, but it should be stated that this alone does not provide sufficient evidence of the nanoparticle shape. Further, each pathway's corresponding surface reaction rate constant $k_{r,n}$ can be evaluated relative to the coverage of the CO species in each pathway (Figures 10E, 10F). Similar to our previous work [Kim preprint] we find no strong dependence on coverage for the slow reaction with under-coordinated sites (pathway 1) at 80 °C. For the fast reaction with the well-coordinated sites (pathway 2) we find a strong linear dependence on the relative coverage of the species which indicates that adsorbate-adsorbate interactions are present, destabilising the adsorbed CO, increasing the rate of reaction at higher coverages. This coverage dependent binding energy of CO has been observed experimentally on Pt(111) single crystals [46], and from DFT simulations of CO covered Pt nanoparticles [47].

8. Conclusion

In summary, we have designed a simplified Temporal Analysis of Products reactor that can be assembled using low-cost and readily available components while still maintaining the majority of the features present in the Gleaves system. Contrary to common thinking, we show that large vacuum chambers and large pumping systems are not required to perform well-defined TAP experiments. When only qualitative kinetic insight is required, less well-defined TAP experiments are possible on systems using even smaller turbomolecular pumps. While the designs outlined in this work lack some of the features of the more commonly used Gleaves systems, we find that precise kinetic, mechanistic, and compositional insight is still feasible with a single-valve system using multi-pulse titration experiments coupled with kinetic modelling. Using the case study of the oxidation of pre-adsorbed CO over 2nm Pt/SiO_2 catalysts, we are able to precisely resolve the composition of sites, and the site and coverage dependent kinetics using a Thin-Zone Multi-Zone TAP Reactor model.

It is our hope that with these systems the barrier to entry to the TAP experiment is significantly decreased, allowing an entirely new generation of researchers to contribute to the field that was first started by John Gleaves over forty years ago.

9. List of Symbols

A	Cross-sectional area of the reactor (cm)
C_A	Concentration of gaseous species A (mol/cm^3)
D_{eA}	Knudsen diffusivity of gas A (cm^2/s)
F_A	Exit flux of gas A (mol/cm^2/s)
F_A^{dim}	Dimensionless exit flux
F_A^{norm}	Normalized exit flux of A (1/s)
N_A	Number of molecules of gas A in the inlet pulse (mol)
S_V	Surface area of catalyst per volume of catalyst (cm^2/cm^3)
$X_{O_2,n}$	Conversion of O_2 from pathway *n*
d_i	Diameter of the interstitial voids (cm)
$k'_{a,n}$	Apparent adsorption/reaction constant for pathway *n*
k_a	Adsorption rate constant (cm^3/mol/s)
k_d	Desorption rate constant (1/s)
$k_{r,n}$	Intrinsic surface reaction constant for pathway *n*
t_A^{dim}	Dimensionless time
t_{max}	Sampling time of the TAP pulse (s)
t_{res}	Mean residence time of gas in the reactor (s)
α_s	Concentration of active sites on the catalyst (cm^2/s)
ε_b	Reactor void fraction
θ_*	Coverage of free sites
θ_A	Coverage of adsorbed species A
L	Reactor length (cm)
M	Molar mass (kg/mol)
T	Temperature (K)
f	Sampling frequency of the pulse response (Hz)
s	Laplace variable
t	Time (s)
z	Axial coordinate of the reactor (cm)
τ	Tortuosity (cm^2/cm^2)

Declaration of Competing Interests

The authors declare that they have no known competing financial interests or personal relationships that could have appeared to influence the work reported in this paper.

Acknowledgements

CR Gratefully acknowledges funding via the Rowland Fellowship though the Rowland Institute at Harvard. CR also would like to acknowledge Rebecca Fushimi, Evgeniy Redekop, John Gleaves, and the entire TAP community for their dedication to the TAP technique and for their consistent guidance over the last 10 years. The authors would also like to acknowledge Samantha Le for generating some replicate data.

References

[1] A. Bruix, J.T. Margraf, M. Andersen, K. Reuter, First-principles-based multiscale modelling of heterogeneous catalysis, Nat. Catal. 2 (2019) 659–670. https://doi.org/10.1038/s41929-019-0298-3.

[2] A.H. Motagamwala, J.A. Dumesic, Microkinetic Modeling: A Tool for Rational Catalyst Design, Chem. Rev. 121 (2021) 1049–1076. https://doi.org/10.1021/acs.chemrev.0c00394.
[3] M.A. Ardagh, O.A. Abdelrahman, P.J. Dauenhauer, Principles of Dynamic Heterogeneous Catalysis: Surface Resonance and Turnover Frequency Response, ACS Catal. 9 (2019) 6929–6937. https://doi.org/10.1021/acscatal.9b01606.
[4] C.T. Campbell, The Degree of Rate Control: A Powerful Tool for Catalysis Research, ACS Catal. 7 (2017) 2770–2779. https://doi.org/10.1021/acscatal.7b00115.
[5] A. Frennet, C. Hubert, Transient kinetics in heterogeneous catalysis by metals, J. Mol. Catal. Chem. 163 (2000) 163–188. https://doi.org/10.1016/S1381-1169(00)00385-X.
[6] C. Ledesma, J. Yang, D. Chen, A. Holmen, Recent approaches in mechanistic and kinetic studies of catalytic reactions using SSITKA technique, ACS Catal. 4 (2014) 4527–4547. https://doi.org/10.1021/cs501264f.
[7] J. Libuda, H.J. Freund, Molecular beam experiments on model catalysts, Surf. Sci. Rep. 57 (2005) 157–298. https://doi.org/10.1016/j.surfrep.2005.03.002.
[8] J.T. Gleaves, G.S. Yablonskii, P. Phanawadee, Y. Schuurman, TAP-2: An interrogative kinetics approach, Appl. Catal. Gen. 160 (1997) 55–88. https://doi.org/10.1016/S0926-860X(97)00124-5.
[9] D. Constales, G.S. Yablonsky, G.B. Marin, J.T. Gleaves, Multi-zone tap-reactors theory and application: I. The global transfer matrix equation, Chem. Eng. Sci. 56 (2001) 133–149. https://doi.org/10.1016/S0009-2509(00)00216-5.
[10] G.S. Yablonsky, M. Olea, G.B. Marin, Temporal analysis of products: Basic principles, applications, and theory, J. Catal. 216 (2003) 120–134. https://doi.org/10.1016/S0021-9517(02)00109-4.
[11] J.T. Gleaves, G. Yablonsky, X. Zheng, R. Fushimi, P.L. Mills, Temporal analysis of products (TAP)-Recent advances in technology for kinetic analysis of multi-component catalysts, J. Mol. Catal. Chem. 315 (2010) 108–134. https://doi.org/10.1016/j.molcata.2009.06.017.
[12] M.A.G. Hevia, A.P. Amrute, T. Schmidt, J. Pérez-Ramírez, Transient mechanistic study of the gas-phase HCl oxidation to Cl2 on bulk and supported RuO2 catalysts, J. Catal. 276 (2010) 141–151. https://doi.org/10.1016/j.jcat.2010.09.009.
[13] C. Reece, E.A. Redekop, S. Karakalos, C.M. Friend, R.J. Madix, Crossing the great divide between single-crystal reactivity and actual catalyst selectivity with pressure transients, Nat. Catal. 1 (2018) 852–859. https://doi.org/10.1038/s41929-018-0167-5.
[14] D. Zhao, X. Tian, D.E. Doronkin, S. Han, V.A. Kondratenko, J.-D. Grunwaldt, A. Perechodjuk, T.H. Vuong, J. Rabeah, R. Eckelt, U. Rodemerck, D. Linke, G. Jiang, H. Jiao, E.V. Kondratenko, In situ formation of ZnOx species for efficient propane dehydrogenation, Nature. 599 (2021) 234–238. https://doi.org/10.1038/s41586-021-03923-3.
[15] K. Morgan, N. Maguire, R. Fushimi, J.T. Gleaves, A. Goguet, M.P. Harold, E.V. Kondratenko, U. Menon, Y. Schuurman, G.S. Yablonsky, Forty years of temporal analysis of products, Catal. Sci. Technol. 7 (2017) 2416–2439. https://doi.org/10.1039/c7cy00678k.
[16] J. Pérez-Ramírez, E.V. Kondratenko, Evolution, achievements, and perspectives of the TAP technique, Catal. Today. 121 (2007) 160–169. https://doi.org/10.1016/j.cattod.2007.01.001.
[17] M. Karatok, R.J. Madix, J.E.S. van der Hoeven, J. Aizenberg, C. Reece, Quantifying oxygen induced surface enrichment of a dilute PdAu alloy catalyst, Catal. Sci. Technol. 11 (2021) 7530–7534. https://doi.org/10.1039/D1CY01337H.
[18] S. Sourav, Y. Wang, D. Kiani, J. Baltrusaitis, R.R. Fushimi, I.E. Wachs, Resolving the Types and Origin of Active Oxygen Species Present in Supported Mn-Na_2WO_4/SiO_2 Catalysts for Oxidative Coupling of Methane, ACS Catal. 11 (2021) 10288–10293. https://doi.org/10.1021/acscatal.1c02315.
[19] T.-S. Kim, C.R. O'Connor, C. Reece, Interrogating Site Dependent Kinetics over SiO2-Supported Pt Nanoparticles, (2023).
[20] J.T. Gleaves, J.R. Ebner, T.C. Kuechler, Temporal Analysis of Products (TAP) — A Unique Catalyst Evaluation System with Submillisecond Time Resolution, Catal. Rev. 30 (1988) 49–116. https://doi.org/10.1080/01614948808078616.

[21] Temporal Analysis of Products (TAP) - Department of Chemistry, (n.d.). https://www.mn.uio.no/kjemi/english/research/groups/catalysis/facilities/tap.html (accessed March 23, 2023).
[22] G.S. Yablonsky, Decoding complexity of chemical reactions, Theor. Found. Chem. Eng. 48 (2014) 608–613. https://doi.org/10.1134/S004057951405025X.
[23] Y. Wang, B. Wang, S. Sourav, R. Batchu, Z. Fang, M.R. Kunz, G. Yablonsky, E. Nikolla, R. Fushimi, Mechanistic pathways and role of oxygen in oxidative coupling of methane derived from transient kinetic studies, Catal. Today. (2022) S0920586122001584. https://doi.org/10.1016/j.cattod.2022.05.004.
[24] S. Sourav, Y. Wang, D. Kiani, J. Baltrusaitis, R.R. Fushimi, I.E. Wachs, New Mechanistic and Reaction Pathway Insights for Oxidative Coupling of Methane (OCM) over Supported Na_2WO_4/SiO_2 Catalysts, Angew. Chem. Int. Ed. 60 (2021) 21502–21511. https://doi.org/10.1002/anie.202108201.
[25] R. Fushimi, Temporal Analysis of Product (TAP), in: Springer Handb. Adv. Catal. Charact., Springer, 2023: pp. 899–934.
[26] A. Goguet, C. Hardacre, N. Maguire, K. Morgan, S.O. Shekhtman, S.P. Thompson, Time of flight mass spectrometry for quantitative data analysis in fast transient studies using a Temporal Analysis of Products (TAP) reactor, Analyst. 136 (2011) 155–163. https://doi.org/10.1039/c0an00435a.
[27] K. Morgan, K.J. Cole, A. Goguet, C. Hardacre, G.J. Hutchings, N. Maguire, S.O. Shekhtman, S.H. Taylor, TAP studies of CO oxidation over CuMnOX and Au/CuMnOX catalysts, J. Catal. 276 (2010) 38–48. https://doi.org/10.1016/j.jcat.2010.08.013.
[28] M.P. Lobera, C. Téllez, J. Herguido, Y. Schuurman, M. Menéndez, TAP studies of Pt–Sn–K/γ-Al2O3 catalyst for propane dehydrogenation, Chem. Eng. J. 171 (2011) 1317–1323. https://doi.org/10.1016/j.cej.2011.05.033.
[29] S.O. Shekhtman, A. Goguet, R. Burch, C. Hardacre, N. Maguire, CO multipulse TAP studies of 2% Pt/CeO2 catalyst: Influence of catalyst pretreatment and temperature on the number of active sites observed, J. Catal. 253 (2008) 303–311. https://doi.org/10.1016/j.jcat.2007.10.028.
[30] Y. Wang, J. Qian, Z. Fang, M.R. Kunz, G. Yablonsky, A. Fortunelli, W.A. Goddard III, R.R. Fushimi, Understanding Reaction Networks through Controlled Approach to Equilibrium Experiments Using Transient Methods, J. Am. Chem. Soc. 143 (2021) 10998–11006. https://doi.org/10.1021/jacs.1c03158.
[31] J.A. Delgado, T.A. Nijhuis, F. Kapteijn, J.A. Moulijn, Modeling of fast pulse responses in the Multitrack: An advanced TAP reactor, Chem. Eng. Sci. 57 (2002) 1835–1847. https://doi.org/10.1016/S0009-2509(02)00071-4.
[32] R. Leppelt, D. Hansgen, D. Widmann, T. Häring, G. Bräth, R.J. Behm, Design and characterization of a temporal analysis of products reactor, Rev. Sci. Instrum. 78 (2007). https://doi.org/10.1063/1.2791948.
[33] Y. Wang, J. Posthuma De Boer, F. Kapteijn, M. Makkee, Next Generation Automotive DeNOx Catalysts: Ceria What Else?, ChemCatChem. 8 (2016) 102–105. https://doi.org/10.1002/cctc.201501038.
[34] L. Scharfenberg, R. Horn, Temporal Analysis of Products Experiments at Atmospheric Pressure: The Epoxidation of Ethylene on Silver, Chem.-Ing.-Tech. 89 (2017) 1350–1359. https://doi.org/10.1002/cite.201700071.
[35] S.O. Shekhtman, G.S. Yablonsky, S. Chen, J.T. Gleaves, Thin-zone TAP-reactor - theory and application, Chem. Eng. Sci. 54 (1999) 4371–4378. https://doi.org/10.1016/S0009-2509(98)00534-X.
[36] M.R. Kunz, R. Batchu, Y. Wang, Z. Fang, G. Yablonsky, D. Constales, J. Pittman, R. Fushimi, Probability theory for inverse diffusion: Extracting the transport/kinetic time-dependence from transient experiments, Chem. Eng. J. 402 (2020) 125985. https://doi.org/10.1016/j.cej.2020.125985.
[37] D. Constales, G.S. Yablonsky, G.B. Marin, J.T. Gleaves, Multi-zone TAP-reactors theory and application. III Multi-response theory and criteria of instantaneousness, Chem. Eng. Sci. 59 (2004) 3725–3736. https://doi.org/10.1016/j.ces.2004.05.023.

[38] S.O. Shekhtman, Interrogative kinetics: A new methodology for catalyst characterization, 2003. https://search.proquest.com/docview/220297257?accountid=12834.
[39] R. Roelant, Mathematical Determination of Reaction Networks from Transient Kinetic Experiments, Universitet Ghent, 2011.
[40] A. Yonge, M.R. Kunz, R. Batchu, Z. Fang, T. Issac, R. Fushimi, A.J. Medford, TAPsolver: A Python package for the simulation and analysis of TAP reactor experiments, Chem. Eng. J. 420 (2021) 129377. https://doi.org/10.1016/j.cej.2021.129377.
[41] D. Proch, T. Trickl, A high-intensity multi-purpose piezoelectric pulsed molecular beam source, Rev. Sci. Instrum. 60 (1989) 713–716. https://doi.org/10.1063/1.1141006.
[42] K. Judai, S. Abbet, A.S. Wörz, M.A. Röttgen, U. Heiz, Turn-over frequencies of catalytic reactions on nanocatalysts measured by pulsed molecular beams and quantitative mass spectrometry, Int. J. Mass Spectrom. 229 (2003) 99–106. https://doi.org/10.1016/S1387-3806(03)00261-6.
[43] Y. Schuurman, Assessment of kinetic modeling procedures of TAP experiments, Catal. Today. 121 (2007) 187–196. https://doi.org/10.1016/j.cattod.2006.06.046.
[44] G.F. Froment, K.B. Bischoff, J. De Wilde, Chemical Reactor Analysis and Design, 3rd Edition, John Wiley & Sons, Incorporated, 2010. https://books.google.com/books?id=lbQbAAAAQBAJ.
[45] D. Constales, G.S. Yablonsky, D.R. D'Hooge, J.W. Thybaut, G.B. Marin, Advanced Data Analysis and Modelling in Chemical Engineering, 2016. https://doi.org/10.1007/s11144-017-1163-5.
[46] G. Ertl, M. Neumann, K.M. Streit, Chemisorption of CO on the Pt(111) surface, Surf. Sci. 64 (1977) 393–410. https://doi.org/10.1016/0039-6028(77)90052-8.
[47] A.D. Allian, K. Takanabe, K.L. Fujdala, X. Hao, T.J. Truex, J. Cai, C. Buda, M. Neurock, E. Iglesia, Chemisorption of CO and mechanism of CO oxidation on supported platinum nanoclusters, J. Am. Chem. Soc. 133 (2011) 4498–4517. https://doi.org/10.1021/ja110073u.